Antiferromagnetic domain walls

N. Papanicolaou
Department of Physics, University of Crete, and Research Center of Crete, Heraklion, Greece
(Received 26 January 1995)

Antiferromagnetic domain walls are shown to exhibit a nonvanishing total magnetic moment. This result is established numerically for a discrete spin system, as well as analytically within a suitable continuum approximation that leads to the nonlinear σ model extended to include anisotropy. The moment is due to certain parity-breaking terms that are implicit in arguments pertaining to the Haldane gap but have been missing in earlier treatments of domain walls. In this paper we present a study of both static and dynamical properties of domain walls in antiferromagnets with an easy-axis anisotropy, but some of the results should prove relevant also for weak ferromagnets.

I. INTRODUCTION

Magnetic domain walls are probably the most concrete examples of topological solitons and have been studied extensively in the case of ferromagnets[1,2] (FM). Much less is known for domain walls in antiferromagnets (AFM) where both a satisfactory theoretical development and actual observation seem to be lacking. But the seeds for an understanding of AFM walls should, in principle, be present in the study of the intermediate case of weak ferromagnets (WFM) where the exchange interaction is antiferromagnetic, while a magnetic moment develops in the ground state due to the Dzyaloshinskii-Moriya anisotropy. Indeed a considerable amount of literature is now available for the description of WFM walls both theoretically and experimentally.[3]

However, when the theoretical results reviewed in Ref. 3 are restricted to vanishing Dzyaloshinskii-Moriya anisotropy and external magnetic field, they lead to the conclusion that the magnetization in an AFM wall vanishes. Such an instance would severely limit the possibility for a direct experimental observation of AFM walls. Nevertheless a proper calculation given in the present paper establishes that the above conclusion is incorrect.

The main theoretical tool used in the study of AFM walls is a reduction of the relevant dynamical equations to a continuum model at the heart of which lies the (relativistic) nonlinear σ model.[4,5] The discrepancy alluded to in the preceding paragraph is simply due to the fact that some of the finer details of such a reduction have been mistreated. In particular, certain terms that emerge in the continuum approximation of the discrete spin model and appear to break spatial parity are absent in the above work. On the other hand, parity-breaking terms are implicit in Haldane's topological arguments for the existence of a mass gap in the excitation spectrum of AFM chains with integer spin.[6,7] We shall show here that such terms are also important for understanding the subject of AFM topological solitons.

To be sure, our main result is established by a direct numerical calculation in the discrete spin model where none of the trickier aspects of the continuum approximation are present. Thus, in Sec. II, static AFM walls are obtained through a relaxation method applied directly on the lattice. We calculate the detailed profile of the wall and find that a nonvanishing total magnetic moment develops for a wide range of couplings of practical interest. A first attempt to understand this result within a continuum approximation is made in Sec. II in preparation for a full description given in Sec. III. Once a consistent continuum model is derived some dynamical questions may readily be addressed. For instance, we calculate the profile of a moving AFM wall which is in turn verified by a numerical simulation in the discrete spin model. The effect of an applied magnetic field is considered in Sec. IV. In the concluding Sec. V we discuss possible phenomenological implications and contemplate generalizations for higher-dimensional solitons, such as antiferromagnetic bubbles, as well as for a more complete understanding of the subject of weak ferromagnets that prompted the present investigation.

II. STATIC DOMAIN WALLS

A domain wall may be viewed either as a one-dimensional (1D) structure within a 3D magnet, in the sense that the spin varies along a single spatial direction, or as a localized soliton within a strictly 1D model. In the bulk of the paper we take the latter view and consider the antiferromagnetic chain described by the Hamiltonian

$$W=\sum_i \left[J(\mathbf{S}_i\cdot\mathbf{S}_{i+1})-\frac{1}{2}g(S_i^3)^2 \right] , \tag{2.1}$$

where the exchange constant J is positive and an easy-axis anisotropy ($g>0$) is introduced in the third direction. The equation of motion for the spin vector $\mathbf{S}_i$ treated as classical may be put in the standard Landau-Lifshitz form

$$\frac{\partial \mathbf{S}_i}{\partial t}=\mathbf{S}_i\times\mathbf{F}_i, \quad \mathbf{S}_i^2=s^2 , \tag{2.2}$$

where s is the constant magnitude of the spin at each lat-

tice site and the effective field $\mathbf{F}_i$ is given by

$$\mathbf{F}_i=-\frac{\partial W}{\partial \mathbf{S}_i}=-J(\mathbf{S}_{i+1}+\mathbf{S}_{i-1})+gS_i^3\mathbf{e}\ , \tag{2.3}$$

where $\mathbf{e}=(0,0,1)$ is a unit vector pointing in the third direction.

In this section, we shall be interested in static solutions which satisfy Eq. (2.2) with the time derivative absent:

$$\mathbf{S}_i\times\mathbf{F}_i=0,\quad \mathbf{S}_i^2=s^2\ . \tag{2.4}$$

The simplest static solution is the usual Néel state which is the lowest-energy state within the classical approximation. Our current task is to examine whether or not there exist stable spin configurations with energy greater than that of the Néel state. An attempt to solve the nonlinear difference equations (2.4) directly is more or less hopeless. We thus invoke a numerical method with a simple physical origin. Suppose that some initial spin configuration evolves according to Eq. (2.2) extended to include dissipation. Then a static solution will eventually be reached as t goes to infinity, which may or may not coincide with the Néel state depending on the choice of the initial condition.

The simplest way to include dissipation in Eq. (2.2) is to write[1,2]

$$\frac{\partial \mathbf{S}_i}{\partial t}+\gamma\left[\mathbf{S}_i\times\frac{\partial \mathbf{S}_i}{\partial t}\right]=\mathbf{S}_i\times\mathbf{F}_i\ , \tag{2.5}$$

where γ is a positive constant. This choice of the dissipative term preserves the spin magnitude s at each lattice site. We may then rewrite Eq. (2.5) in a form more suitable for computation, namely

$$(1+\gamma^2s^2)\frac{\partial \mathbf{S}_i}{\partial t}=(\mathbf{S}_i\times\mathbf{F}_i)-\gamma[\mathbf{S}_i\times(\mathbf{S}_i\times\mathbf{F}_i)]\ . \tag{2.6}$$

Since our goal in this section is to obtain static solutions we can accelerate the process by using Eq. (2.6) with a very large dissipation constant γ. Then the first (precession) term may be neglected and the dissipation constant itself may be eliminated by a suitable rescaling of the time variable. We thus arrive at the fully dissipative equation

$$\frac{\partial \mathbf{S}_i}{\partial t}=-\mathbf{S}_i\times(\mathbf{S}_i\times\mathbf{F}_i)\ , \tag{2.7}$$

which will be the basis for our numerical simulation of static solutions. It is not difficult to see that the energy W is a monotonically decreasing function of time when the spin evolves according to either Eq. (2.6) or (2.7). The advantage of (2.7) is that it suppresses transients and rapidly leads to equilibrium.

If an initial spin configuration is chosen more or less at random, it will likely be driven by Eq. (2.7) to the Néel state. However judicious choices of the initial condition may lead to nontrivial static solutions such as domain walls. To motivate the existence of AFM domain walls we consider for the moment a finite open chain with an even number of sites $\Lambda=2N$, where N is also even; these restrictions will not be essential in a sense made precise later in this section. Now suppose that the first half of the chain consisting of N sites is set in a Néel state with its first spin pointing up and its last one down. The second half of the chain is also chosen to be in a Néel state but its first spin points down and the last one up. Hence the full chain is almost everywhere in a Néel state except for a defect in its middle where two neighboring spins point in the same direction. Such a configuration is the prototype for an AFM domain wall and is actually an exact solution which is stable when the dimensionless ratio

$$\varepsilon=\sqrt{g/J} \tag{2.8}$$

exceeds a certain critical value. However for most values of ε of practical interest ($\varepsilon\lesssim 1$) the prototype AFM wall is unstable in that a small randomness in the directions of the two middle spins would spread out until a stable domain-wall configuration is reached whose details depend on the specific value of ε and its (half) width is given roughly by $1/\varepsilon$. In all cases, an initial configuration prepared in the manner described above would not be driven to the Néel state provided that the chain is sufficiently long ($\Lambda\gg 1/\varepsilon$).

In our simulations we used an open chain with $\Lambda=2\,000$ sites and a first-order time-differencing scheme which proved to be very stable if the time step is chosen in the neighborhood of $\delta t\sim 10^{-2}$. We further used a variety of initial configurations retaining only the essential topological characteristics of the prototype wall, but observed a rapid convergence to a static AFM wall which is independent of the initial configuration. Having thus described the algorithm the remainder of this section is devoted to a detailed discussion of explicit results.

We begin with $\varepsilon=1/2$ for which the calculated wall is illustrated at every site of a limited portion of the lattice in Fig. 1. The wall is very narrow for this large value of ε in the sense that significant deviations from the Néel state occur only over a few lattice sites around the wall center. Nevertheless the essential features of AFM domain walls are already apparent in Fig. 1. First we note the simple fact that one of the spin components in the (12) plane

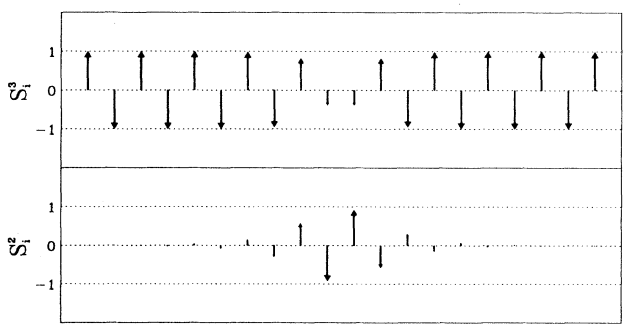

FIG. 1. A static AFM domain wall illustrated through the spin components $S_i^1=0$, S_i^2, and S_i^3 at each lattice site i of a limited portion of the lattice around the wall center. The wall is rather narrow due to the large anisotropy used in the corresponding numerical calculation ($\varepsilon=1/2$).

vanishes; because of the azimuthal symmetry the vanishing component is chosen to be S_i^1 without loss of generality. A more interesting property that can also be discerned from Fig. 1 is that the total magnetic moment

$$\boldsymbol{\mu}=\sum_{i=1}^{\Lambda}\mathbf{S}_i \tag{2.9}$$

is nonvanishing in spite of the generally observed sign alternation at consecutive sites. An explicit computation of $\boldsymbol{\mu}=(\mu_1,\mu_2,\mu_3)$ for $\varepsilon=1/2$ yields $\mu_1=0=\mu_2$ and $\mu_3/s=0.995\,612\,66$. Thus we arrive at the important conclusion that a net moment develops in the third direction with a magnitude comparable to that of the local (staggered) moment s.

In view of the somewhat surprising nature of the above result we have repeated the calculation for a wide range of values of ε and the results are tabulated in Table I. Clearly the total moment reaches the value s for small ε with rapidly increasing accuracy. Essential deviations from this value occur only for strong anisotropy, $\varepsilon\sim 1$, where the wall size reduces to a few lattice spacings. For even stronger anisotropy the total moment vanishes, while the wall structure reduces to that of the prototype AFM wall used to motivate our results. In fact, the numerical simulation indicates that a critical value exists, in the region $1.1<\varepsilon<1.2$, after which the prototype wall becomes stable. We shall not pursue this critical transition further but concentrate on the weak-anisotropy region where the domain walls acquire macroscopic size and are likely to be more important for practical purposes.

First we comment on a minor technical assumption made earlier in this section. Once a domain wall is realized on an open chain with an even number of sites $\Lambda=2N$ one may remove one or more spins from either side of the chain without affecting the stability of the wall provided that $\Lambda\gg 1/\varepsilon$. The wall may unwind and become the Néel state only when $\Lambda\sim 1/\varepsilon$. These facts are easily established by reapplying the relaxation algorithm after one or more spins are removed.

TABLE I. Numerical results for the total moment ($\mu_1=0=\mu_2,\mu_3\neq 0$) of a static AFM domain wall as a function of anisotropy.

$\varepsilon=\sqrt{g/J}$	μ_3/s
0.1	1.000 000 00
0.2	1.000 000 00
0.3	0.999 989 85
0.4	0.999 536 55
0.5	0.995 612 66
0.6	0.980 786 53
0.7	0.944 997 98
0.8	0.877 185 77
0.9	0.763 064 21
1.0	0.577 768 28
1.1	0.267 165 36
1.2	0.000 000 00

Thus we turn to the discussion of macroscopic domain walls, which occur at weak anisotropy, and eventually make contact with the continuum limit of an antiferromagnet. In searching for variables that may possess such a limit one usually groups the sites of the original chain $i=1,2,\ldots,\Lambda=2N$ into the pairs $(12),(34),\ldots,(\Lambda-1,\Lambda)$. One may then label each pair by a Greek index $\alpha=1,2,\ldots,N$ which will be referred to as the sublattice index. The pair with index α carries the two spins $\mathbf{S}_{2\alpha-1}$ and $\mathbf{S}_{2\alpha}$, or their linear combinations

$$\mathbf{m}_\alpha=\frac{1}{2s}(\mathbf{S}_{2\alpha-1}+\mathbf{S}_{2\alpha}),\quad \mathbf{n}_\alpha=\frac{1}{2s}(\mathbf{S}_{2\alpha-1}-\mathbf{S}_{2\alpha})\ . \tag{2.10}$$

The constraint $\mathbf{S}_i^2=s^2$ satisfied by the original spin for each lattice index i is then translated into two constraints for each sublattice index α, namely

$$\mathbf{m}_\alpha\cdot\mathbf{n}_\alpha=0,\quad \mathbf{m}_\alpha^2+\mathbf{n}_\alpha^2=1\ . \tag{2.11}$$

It is evident from definition (2.10) that the vector $\mathbf{m}$ plays the role of the magnetization density. In particular, the total moment defined in Eq. (2.9) may be rewritten as

$$\boldsymbol{\mu}=2s\sum_{\alpha=1}^{N}\mathbf{m}_\alpha\ . \tag{2.12}$$

Both the local moment $\mathbf{m}$ and the total one $\boldsymbol{\mu}$ vanish in a pure Néel state but do not do so in an AFM wall. The physical significance of the vector $\mathbf{n}$ is more subtle.

The basic assumption of all earlier treatments[3–7] is that the variables $\mathbf{m}$ and $\mathbf{n}$ possess smooth continuum limits. We now check this assumption using our explicit numerical results for small values of ε for which an AFM wall extends over a significant number of lattice sites. Once the spins $\mathbf{S}_i$ have been computed by the relaxation algorithm they are combined into the variables $\mathbf{m}$ and $\mathbf{n}$ of Eq. (2.10) and then plotted as functions of the variable

$$x=2\varepsilon(\alpha-\alpha_0)\ , \tag{2.13}$$

where α is the integer-valued sublattice index and α_0 is an arbitrary constant that sets the origin of the coordinate system. In our explicit illustrations we set the origin at the wall center which is, in turn, placed at the middle of the chain so that $\alpha_0=(N+1)/2$; but the location of the wall is clearly arbitrary as long as it stays sufficiently apart from the endpoints of the open chain. Now the dimensionless discrete variable x of Eq. (2.13) becomes continuous in the limit $\varepsilon\to 0$ and provides a measure of position along the original chain. The actual distance on the chain is given by xa/ε where a is the lattice spacing. However the lattice constant a need not be used in any step of the theoretical development, as is done throughout this paper, except when quantities such as distance, velocity, etc., have to be translated in physical units.

In Fig. 2 we use the specific value $\varepsilon=0.1$ and join the discrete points in the graph by the interpolation algorithm of the graphics routine. It is evident that a smooth continuum emerges for the variables $\mathbf{m}$ and $\mathbf{n}$ even for this relatively large value of ε. The important features of Fig. 2 other than continuity are (i) the vector $\mathbf{n}$ exhibits

the standard domain-wall structure and (ii) a nonvanishing magnetization density $\mathbf{m}$ develops within the wall which appears to be proportional to the gradient of the field $\mathbf{n}$. To establish this fact we now derive explicitly the continuum limit of an AFM wall using an indirect method which applies only to static solutions but is very illuminating. A more formal as well as complete derivation is discussed in Sec. III.

The indirect method is based on the simple observation that a static AFM wall may be obtained from the corresponding FM one by the relation

$$\mathbf{S}_i^{\mathrm{AFM}}=(-1)^i\mathbf{S}_i^{\mathrm{FM}} . \tag{2.14}$$

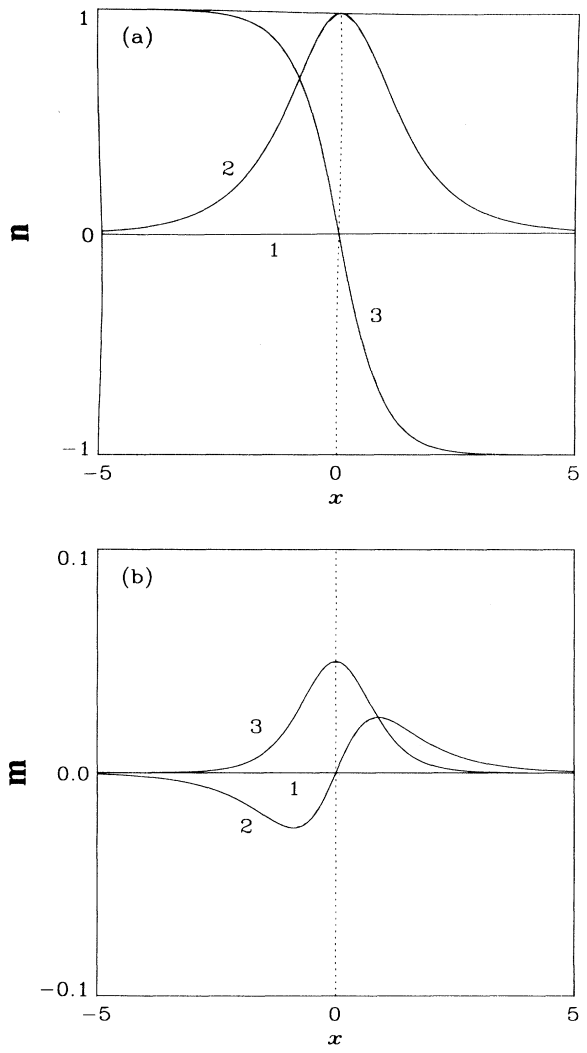

FIG. 2. A static AFM domain wall illustrated through the three components of (a) the vector $\mathbf{n}=(n_1,n_2,n_3)$ and (b) the magnetization density $\mathbf{m}=(m_1,m_2,m_3)$. Dashed lines correspond to the results of a numerical calculation in the discrete spin model with $\varepsilon=0.1$ but are difficult to distinguish from the solid lines depicting the continuum solution [(2.15) and (2.16)].

Indeed if $\mathbf{S}_i^{\mathrm{AFM}}$ satisfies the static Eq. (2.4) with exchange constant J then $\mathbf{S}_i^{\mathrm{FM}}$ given by Eq. (2.14) satisfies the same equation with exchange constant $-J$. It should be stressed that the above property is not valid for the full equation of motion (2.2). However Eq. (2.14) is sufficient to derive the continuum limit of a static AFM wall.

Hence using the well-known continuum expression for a FM wall, which is viewed as an approximation of the discrete solution at small ε, one may construct the corresponding approximate solution for an AFM wall from Eq. (2.14) and then calculate the vectors $\mathbf{m}$ and $\mathbf{n}$ from Eq. (2.10). We omit here the technical details and state the final results. The vector $\mathbf{n}=(n_1,n_2,n_3)$ is given by

$$n_1=0, \quad n_2=\frac{1}{\cosh x}, \quad n_3=-\tanh x , \tag{2.15}$$

where x is the dimensionless position variable of Eq. (2.13) and terms of order ε^2 and higher have been omitted. The magnetization density $\mathbf{m}=(m_1,m_2,m_3)$ is accordingly given in the leading approximation by

$$m_1=0, \quad m_2=\frac{\varepsilon}{2}\frac{\tanh x}{\cosh x}, \quad m_3=\frac{\varepsilon}{2}\frac{1}{\cosh^2 x} , \tag{2.16}$$

or by the general formula

$$\mathbf{m}=-\frac{\varepsilon}{2}\mathbf{n}' , \tag{2.17}$$

where the prime denotes differentiation with respect to x. From the point of view of the corresponding FM wall the validity of the above formula is more or less obvious, for it reflects the fact that the difference of the values of the spin at two consecutive sites is proportional to its derivative in the limit of small ε. The explicit expressions (2.15) and (2.16) are also plotted in Fig. 2 and are graphically indistinguishable from our earlier results obtained in the discrete spin model, even for the relatively large value $\varepsilon=0.1$ used in our illustration.

An important element of the preceding discussion is Eq. (2.17) which relates the magnetization density $\mathbf{m}$ to the gradient of the field $\mathbf{n}$. This relation explains without a detailed calculation why a nonvanishing moment occurs within an AFM wall. The total moment is given by Eq. (2.12) whose continuum ($\varepsilon\to 0$) limit reads

$$\boldsymbol{\mu}=\frac{2s}{2\varepsilon}\int dx\,\mathbf{m}=-\frac{s}{2}\int dx\,\mathbf{n}' , \tag{2.18}$$

or

$$\boldsymbol{\mu}=-\frac{s}{2}[\mathbf{n}(+\infty)-\mathbf{n}(-\infty)] . \tag{2.19}$$

Therefore the total moment is related to the asymptotic values of the field $\mathbf{n}$. Because the latter exhibits a domain-wall structure, with $\mathbf{n}(\mp\infty)=(0,0,\pm 1)$, Eq. (2.19) yields $\boldsymbol{\mu}=(\mu_1,\mu_2,\mu_3)$ with

$$\mu_1=0=\mu_2, \quad \mu_3=s . \tag{2.20}$$

This is precisely the result obtained through the numerical simulation at small values of ε (see Table I).

III. MOVING DOMAIN WALLS

In discussing the dynamics we reverse the logic of the preceding section and consider first the continuum approximation of Eq. (2.2). Once the basic results have been obtained we shall verify them by a numerical calculation in the discrete spin model.

The mapping to the ferromagnetic chain given by Eq. (2.14) is no longer valid for time-dependent fields. We thus derive the continuum limit of Eq. (2.2) by a more direct treatment which should contain the results of Sec. II as a special case. The derivation is formal but clearly illustrates the assumptions underlying the existence of a smooth continuum limit in an antiferromagnet. Hence we return to the labeling of sites discussed in connection with Eq. (2.10) and introduce the convenient notation

$$\mathbf{A}_\alpha=\mathbf{S}_{2\alpha-1},\quad \mathbf{B}_\alpha=\mathbf{S}_{2\alpha} \tag{3.1}$$

for the two spins contained in a pair of sites labeled by the sublattice index α. Equation (2.2) applied for $i=1,2,\ldots,\Lambda=2N$ is equivalent to the system of equations

$$\begin{aligned}\frac{\partial \mathbf{A}_\alpha}{\partial t}&=\mathbf{A}_\alpha\times[-J(\mathbf{B}_\alpha+\mathbf{B}_{\alpha-1})+gA_\alpha^3\mathbf{e}]\ ,\\ \frac{\partial \mathbf{B}_\alpha}{\partial t}&=\mathbf{B}_\alpha\times[-J(\mathbf{A}_\alpha+\mathbf{A}_{\alpha+1})+gB_\alpha^3\mathbf{e}]\ ,\end{aligned} \tag{3.2}$$

applied for $\alpha=1,2,\ldots,N$. The main assumption is that the spin variables $\mathbf{A}_\alpha$ and $\mathbf{B}_\alpha$ approach continuum limits on each sublattice, when $\varepsilon\to 0$, which we denote by $\mathbf{A}=\mathbf{A}(x)$ and $\mathbf{B}=\mathbf{B}(x)$ where x may still be chosen the dimensionless position variable of Eq. (2.13). Then we make the replacements $\mathbf{A}_\alpha\to\mathbf{A}$ and $\mathbf{B}_\alpha\to\mathbf{B}$ in Eq. (3.2) together with

$$\begin{aligned}\mathbf{A}_{\alpha+1}&\to\mathbf{A}+(2\varepsilon)\mathbf{A}'+\tfrac{1}{2}(2\varepsilon)^2\mathbf{A}''\ ,\\ \mathbf{B}_{\alpha-1}&\to\mathbf{B}-(2\varepsilon)\mathbf{B}'+\tfrac{1}{2}(2\varepsilon)^2\mathbf{B}''\ ,\end{aligned} \tag{3.3}$$

to obtain

$$\begin{aligned}\frac{1}{2J}\frac{\partial \mathbf{A}}{\partial t}&=\mathbf{A}\times\left[-\mathbf{B}+\varepsilon\mathbf{B}'-\varepsilon^2\mathbf{B}''+\frac{1}{2}\varepsilon^2A_3\mathbf{e}\right]\ ,\\ \frac{1}{2J}\frac{\partial \mathbf{B}}{\partial t}&=\mathbf{B}\times\left[-\mathbf{A}-\varepsilon\mathbf{A}'-\varepsilon^2\mathbf{A}''+\frac{1}{2}\varepsilon^2B_3\mathbf{e}\right]\ ,\end{aligned} \tag{3.4}$$

where we have also expressed the anisotropy constant g in terms of ε through Eq. (2.8) and A_3, B_3 are the third components of the respective fields.

One of the surprising properties of Eqs. (3.4) is that symmetry under parity, $x\to -x$, is actually reduced to symmetry under the combined transformation

$$x\to -x,\quad \mathbf{A}\leftrightarrow\mathbf{B}\ . \tag{3.5}$$

However such a property must be interpreted with caution because system (3.4) is not yet fully consistent for two related reasons. First, it appears to mix terms with different powers of the small parameter ε. Second, once memory of site counting is lost in the continuum limit, the number of independent fields seems to have been doubled in Eqs. (3.4).

In order to derive a consistent set of equations it is convenient to work with the variables $\mathbf{m}$ and $\mathbf{n}$ of Eq. (2.10) or

$$\mathbf{m}=\frac{1}{2s}(\mathbf{A}+\mathbf{B}),\quad \mathbf{n}=\frac{1}{2s}(\mathbf{A}-\mathbf{B})\ , \tag{3.6}$$

which satisfy the constraints

$$\mathbf{m}\cdot\mathbf{n}=0,\quad \mathbf{m}^2+\mathbf{n}^2=1\ . \tag{3.7}$$

We also introduce the dimensionless time variable

$$\tau=2\varepsilon sJt\ , \tag{3.8}$$

which shares with the dimensionless position variable x of Eq. (2.13) the property that they are both linear in the parameter ε, as suggested by the fact that the semiclassical dispersion of spin-wave excitations in the isotropic chain,

$$\omega_k=2sJ|\sin k|\ , \tag{3.9}$$

is linear in the wave number k in the long-wavelength limit.

System (3.4) is then rewritten as

$$\begin{aligned}\varepsilon\frac{\partial \mathbf{m}}{\partial\tau}&=[-\varepsilon(\mathbf{m}\times\mathbf{n})+\varepsilon^2(\mathbf{n}\times\mathbf{n}'-\mathbf{m}\times\mathbf{m}')]'\\ &\quad+\frac{1}{2}\varepsilon^2[m_3(\mathbf{m}\times\mathbf{e})+n_3(\mathbf{n}\times\mathbf{e})]\ ,\\ \varepsilon\frac{\partial \mathbf{n}}{\partial\tau}&=2(\mathbf{m}\times\mathbf{n})+\varepsilon(\mathbf{m}\times\mathbf{m}'-\mathbf{n}\times\mathbf{n}')\\ &\quad+\varepsilon^2(\mathbf{m}\times\mathbf{n}''+\mathbf{m}''\times\mathbf{n})\\ &\quad+\frac{1}{2}\varepsilon^2[n_3(\mathbf{m}\times\mathbf{e})+m_3(\mathbf{n}\times\mathbf{e})]\ .\end{aligned} \tag{3.10}$$

A simple inspection of these equations suggests that consistency is obtained if $\mathbf{m}$ is of order ε. Then the leading approximation of the second equation is given by

$$\varepsilon\frac{\partial \mathbf{n}}{\partial\tau}=2(\mathbf{m}\times\mathbf{n})-\varepsilon(\mathbf{n}\times\mathbf{n}') \tag{3.11}$$

and the constraints (3.7) reduce to

$$\mathbf{m}\cdot\mathbf{n}=0,\quad \mathbf{n}^2=1\ , \tag{3.12}$$

to within terms of order ε^2. Therefore taking the cross product of both sides of Eq. (3.11) with $\mathbf{n}$ and using the constraints (3.12) yields

$$\mathbf{m}=\frac{\varepsilon}{2}[-\mathbf{n}'+(\mathbf{n}\times\dot{\mathbf{n}})]\ , \tag{3.13}$$

where the prime denotes differentiation with respect to the position variable x of Eq. (2.13) and the dot with respect to the time variable τ of Eq. (3.8). Equation (3.13) is finally introduced in the first of Eqs. (3.10) to yield in the limit $\varepsilon\to 0$

$$\mathbf{n}\times(\ddot{\mathbf{n}}-\mathbf{n}''-n_3\mathbf{e})=0\ . \tag{3.14}$$

Equations (3.13) and (3.14) supplemented by the constraints (3.12) constitute the sought after continuum limit

of the equation of motion (2.2) appropriate for the description of an antiferromagnetic chain.

It should be noted that the magnetization density **m** is no longer an independent dynamical variable but is expressed entirely in terms of the field **n** through Eq. (3.13) which is a generalization of Eq. (2.17) obtained earlier for static solutions. Since Eq. (3.14) is invariant under the ordinary parity transformation $x \to -x$, all parity-breaking contributions are now contained in the gradient term of Eq. (3.13) which is invariant only under the restricted parity transformation (3.5), or

$$x \to -x, \quad \mathbf{m} \to \mathbf{m}, \quad \mathbf{n} \to -\mathbf{n} . \tag{3.15}$$

We should add here that such a term is missing in earlier treatments, even though a dynamical contribution proportional to $\mathbf{n} \times \dot{\mathbf{n}}$ does appear in Eq. (2.28) of Ref. 3.

Thus the dynamics is governed by Eq. (3.14) which is a simple generalization of the relativistic nonlinear σ model to include anisotropy. The corresponding "velocity of light" is equal to unity thanks to our choice of rationalized space and time variables. At this point one may restore actual distances measured by xa/ε where a is the lattice spacing on the original chain. Also taking into account the definition of the time variable τ in Eq. (3.8), we conclude that velocity is measured in units of $c = 2asJ$ which is the group velocity of spin-wave excitations in the isotropic chain, in the long-wavelength limit; see Eq. (3.9) applied for small k. For typical values of the local moment ($s \sim \hbar$), of the exchange constant ($Js^2 \sim 10$ K), and of the lattice constant ($a \sim 4 \times 10^{-10}$ m) one finds that $c \sim 10^3$ m/sec.

As a first application of the preceding results we rederive the static AFM wall discussed in Sec. II. Equation (3.14) reduces to

$$\mathbf{n} \times (\mathbf{n}'' + n_3 \mathbf{e}) = 0 , \tag{3.16}$$

which is solved by an ansatz of the form

$$\mathbf{n} = (0, \sin\theta, \cos\theta) , \tag{3.17}$$

provided that the angle θ satisfies the ordinary differential equation

$$\theta'' = \cos\theta \sin\theta . \tag{3.18}$$

An explicit solution of this equation is given by

$$\sin\theta = \frac{1}{\cosh x}, \quad \cos\theta = -\tanh x , \tag{3.19}$$

thus reproducing Eq. (2.15). The magnetization density **m** is then computed from Eq. (3.13), with the dynamical term absent, thus recovering Eq. (2.16). One should add that a solution is obtained also by changing the sign of $\cos\theta$ in Eq. (3.19) leading to two versions of an AFM wall distinguished by the asymptotic values of the field **n** (kink and antikink). This additional possibility together with AFM walls obtained by a trivial azimuthal rotation will not be mentioned further in the remainder of the paper.

We may now go farther and compute explicitly the profile of an AFM wall moving with an arbitrary velocity $v < 1 (= c)$. The field **n** is obtained simply by a Lorentz transformation of the static solution (3.19), i.e.,

$$n_1 = 0, \quad n_2 = \frac{1}{\cosh u}, \quad n_3 = -\tanh u , \tag{3.20}$$

where

$$u = \frac{x - v\tau}{\sqrt{1 - v^2}} . \tag{3.21}$$

The magnetization density **m** is calculated from Eq. (3.13) noting that both the gradient and the dynamical term are now important:

$$m_1 = \frac{\varepsilon v}{2\sqrt{1-v^2}} \frac{1}{\cosh u}, \quad m_2 = \frac{\varepsilon}{2\sqrt{1-v^2}} \frac{\tanh u}{\cosh u} , \quad m_3 = \frac{\varepsilon}{2\sqrt{1-v^2}} \frac{1}{\cosh^2 u} . \tag{3.22}$$

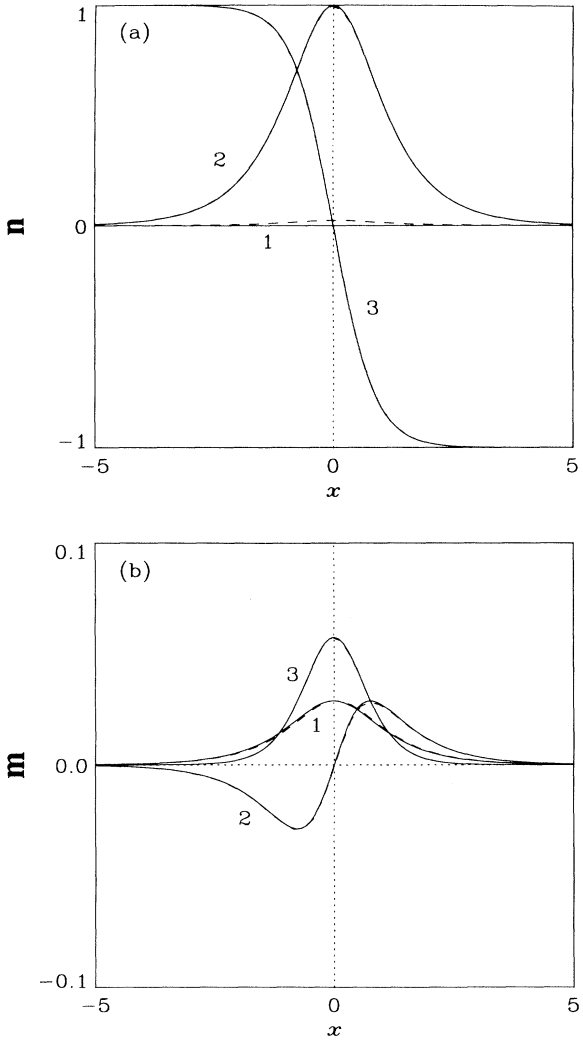

FIG. 3. A moving AFM domain wall illustrated through the vector **n** and the magnetization density **m**. Solid lines depict the continuum solution [(3.20)–(3.22)] which is found to be in satisfactory agreement with a numerical calculation (dashed lines) for $\varepsilon = 0.1$ and $v = 1/2$ described in Sec. III.

A notable feature of this result is that a nonvanishing component develops in the first direction, for $v \neq 0$, due to the dynamical term in Eq. (3.13). We further compute the total moment of the wall by a relation analogous to Eq. (2.18):

$$\mu = \frac{s}{\varepsilon} \int dx\, \mathbf{m} = (\mu_1, \mu_2, \mu_3) , \tag{3.23}$$

with

$$\mu_1 = \frac{1}{2} \pi v s , \quad \mu_2 = 0 , \quad \mu_3 = s . \tag{3.24}$$

Therefore the total moment in the third direction remains the same with that of a static AFM wall, but a net moment develops also in the first direction which acquires its maximum value ($\pi s/2$) in the extreme relativistic limit ($v \to 1$).

In view of the formal nature of the derivation of the continuum limit given above, it is certainly desirable to carry out a direct numerical verification of the main results within the discrete spin model. Suppose that the original equation of motion (2.2) is solved with an initial condition furnished by the continuum approximation. Specifically, Eqs. (3.20)–(3.22) are used to calculate the initial ($\tau = 0$) values of the fields $\mathbf{m}$ and $\mathbf{n}$ for the discrete set of points $x = 2\varepsilon(\alpha - \alpha_0)$ of Eq. (2.13), which are inserted in Eq. (2.10) to obtain the original spin variables $\mathbf{S}_{2\alpha-1}$ and $\mathbf{S}_{2\alpha}$. This initial configuration is then evolved according to Eq. (2.2) solved numerically. After any given time interval the obtained new spin configuration is used to recalculate the fields $\mathbf{m}$ and $\mathbf{n}$ from Eq. (2.10) which are again plotted as functions of the discrete variable x but with points in the graph joined smoothly through the graphics routine.

The continuum approximation of the moving wall given in Eqs. (3.20)–(3.22) will have been verified if the solution of Eq. (2.2) described in the preceding paragraph produces a wall structure that proceeds rigidly with a constant velocity equal to the input one v; i.e., if the wall retains its initial profile except for an overall displacement equal to $v\tau$. Indeed a numerical solution for the specific parameters $\varepsilon = 0.1$ and $v = 1/2$ verifies the above picture. For instance, in Fig. 3, we depict the initial configuration together with the one obtained numerically after the wall had moved with a constant velocity $v \approx 1/2$ about ten times its width, using a common origin that coincides with the wall centers. The agreement is very satisfactory in view of the relatively large values of ε and v used in this numerical experiment. The continuum approximation improves rapidly for smaller values of ε and v, while it breaks down for parameters such that either ε is large ($\varepsilon \sim 1$) or v approaches a narrow region near the magnon velocity ($v \sim 1$); in either case the wall width reduces to a few lattice spacings. Therefore the continuum approximation remains valid for most parameters of practical interest.

IV. RESPONSE TO EXTERNAL FIELDS

Probing with external fields has been one of the basic tools in studying the dynamics of magnetic domain walls.[1–3] An analytical solution due to Walker[8] describes a FM wall driven by an applied uniform magnetic field H in the presence of dissipation. The wall reaches a steady state with a terminal velocity $v = v(H)$ provided that the field is smaller than a certain critical value H_W; it undergoes a complicated (oscillatory) evolution for $H > H_W$. Although the Walker solution applies only to ideal FM walls, in the sense that important effects due to finite film thickness are neglected, it has been a source of intuition for most treatments of domain-wall dynamics.[1,2] The situation is less clear in the case of weak ferromagnets but a number of interesting results is also available.[3]

Unfortunately an AFM wall cannot be driven by a uniform field because of the lack of a domain-wall structure in the magnetization density $\mathbf{m}$ computed in earlier sections. Instead an applied field sets an AFM wall in a precession mode which eventually degenerates, if dissipation is present, to a static wall modified by the external field. The latter affects also the ground (Néel) state which becomes, in general, a canted AFM state. The corresponding domain walls may then be viewed as topological defects within an otherwise uniform canted state. The main objective of this section is to provide an explicit calculation of such defects.

The external magnetic field $\mathbf{H}$ may be accounted for simply by replacing the effective field $\mathbf{F}_i$ of Eq. (2.3) with

$$\mathbf{F}_i \to \mathbf{F}_i + g_0 \mu_0 \mathbf{H} , \tag{4.1}$$

where g_0 is the gyromagnetic ratio and $\mu_0 = e/2m_e c$ is the Bohr magneton divided by the Planck constant $\hbar$. In our theoretical calculations it proves convenient to work with the dimensionless field

$$\mathbf{h} = \frac{g_0 \mu_0 \mathbf{H}}{2\varepsilon s J} , \tag{4.2}$$

a definition that resembles the rescaling of time given in Eq. (3.8). Using a gyromagnetic ratio $g_0 = 2$ in our standard example, where $s = \hbar$ and $Js^2 = 10$ K, one finds that $2sJ/g_0\mu_0 = 15 \times 10^4$ G. This value may be employed in conjunction with a specific (dimensionless) anisotropy constant $\varepsilon = \sqrt{g/J}$ in order to translate the field $\mathbf{h}$ in physical units.

As in Sec. III, we shall let the continuum approximation guide us through the main results which will then be checked with a numerical calculation in the discrete spin model. The burden on the continuum approximation is now increased by the fact that the applied field introduces a new scale in the problem. The specific choice of the rescaled field $\mathbf{h}$ made in Eq. (4.2) was motivated by the requirement $Ht \sim h\tau$, so that precession effects are treated reasonably in the limit $\varepsilon \to 0$.

Otherwise the derivation is similar to that of Sec. III, including an additional term $\varepsilon(\mathbf{m} \times \mathbf{h})$ in the first equation of (3.10) and $\varepsilon(\mathbf{n} \times \mathbf{h})$ in the second one. The magnetization density $\mathbf{m}$ is then expressed in terms of $\mathbf{n}$ by

$$\mathbf{m} = \frac{\varepsilon}{2} [-\mathbf{n}' + (\mathbf{n} \times \dot{\mathbf{n}}) - \mathbf{n} \times (\mathbf{n} \times \mathbf{h})] , \tag{4.3}$$

and $\mathbf{n}$ itself satisfies the differential equation

$$\mathbf{n}\times[\ddot{\mathbf{n}}-\mathbf{n}''-n_3\mathbf{e}+(\mathbf{n}\cdot\mathbf{h})\mathbf{h}+2(\mathbf{h}\times\dot{\mathbf{n}})]=0\ , \tag{4.4}$$

thus generalizing Eqs. (3.13) and (3.14) to include the effect of a uniform, time-independent magnetic field $\mathbf{h}$. One of the notable features of this result is that Lorentz invariance is now broken.[3] One should add that the algebraic constraints satisfied by $\mathbf{m}$ and $\mathbf{n}$ remain the same with those of Eq. (3.12).

We shall mostly discuss static solutions which satisfy the reduced system

$$\mathbf{m}=-\frac{\varepsilon}{2}[\mathbf{n}'+\mathbf{n}\times(\mathbf{n}\times\mathbf{h})] \tag{4.5}$$

and

$$\mathbf{n}\times[\mathbf{n}''+n_3\mathbf{e}-(\mathbf{n}\cdot\mathbf{h})\mathbf{h}]=0\ . \tag{4.6}$$

At this point one must also specify the direction of the applied field. We consider first the case of an in-plane field, i.e.,

$$\mathbf{h}=(0,h,0)\ , \tag{4.7}$$

which is taken to point along the second axis without loss of generality thanks to the azimuthal symmetry. Equation (4.6) is again solved by an ansatz of the form (3.17) provided that the angle θ satisfies the equation

$$\theta''=(1+h^2)\cos\theta\sin\theta\ , \tag{4.8}$$

which differs from Eq. (3.18) only by a rescaling of the coordinate x. The desired solution of Eq. (4.6) is then given by

$$n_1=0,\quad n_2=\frac{1}{\cosh y},\quad n_3=-\tanh y\ , \tag{4.9}$$

with $y=\sqrt{1+h^2}x$, and the magnetization density calculated from Eq. (4.5) reads

$$m_1=0,\quad m_2=\frac{\varepsilon}{2}\left[h\tanh^2 y+\sqrt{1+h^2}\frac{\tanh y}{\cosh y}\right],$$
$$m_3=\frac{\varepsilon}{2}\left[h\frac{\tanh y}{\cosh y}+\frac{\sqrt{1+h^2}}{\cosh^2 y}\right]. \tag{4.10}$$

The asymptotic values in the limits $x\to\mp\infty$,

$$\mathbf{n}(\mp\infty)=(0,0,\pm1),\quad \mathbf{m}(\mp\infty)=(0,\varepsilon h/2,0)\ , \tag{4.11}$$

demonstrate that the field $\mathbf{n}$ exhibits the standard domain-wall structure and a nonvanishing magnetization develops even in the ground state.

It is now important to make contact with the discrete model. First we perform a simulation along the lines suggested by the introductory remarks of this section. The (discrete) static AFM wall calculated in Sec. II is subjected to a uniform in-plane field which is turned on at $t=0$. The numerical task consists of solving the initial-value problem for the discrete evolution equation (2.6) extended to include the applied field according to Eq. (4.1). If some dissipation is present ($\gamma\neq0$) precession effects are suppressed at sufficiently long time intervals and the spin configuration reaches a static solution which should be the discrete analog of the continuum solution [(4.9) and (4.10)]. Here we will not discuss the intermediate details of the time evolution but merely the resulting static configuration; hence the process can be accelerated by using the fully dissipative equation (2.7) also extended according to Eq. (4.1). The results of this numerical experiment are shown in Fig. 4 together with the continuum solution [(4.9) and (4.10)] for the specific parameters $\varepsilon=0.1$ and $h=1/2$. The observed agreement is again very good. Nevertheless the continuum approximation is expected to deteriorate for larger values of the applied field, at any given ε, as is suggested by the fact that the width of the calculated wall decreases with increasing field h.

Some information on the range of validity of the continuum approximation in the presence of an external field can be surmised already from a consideration of the classical ground state in the discrete spin model. In a simple generalization of the Néel state the spin assumes only two distinct values, one for each sublattice, which we denote by $\mathbf{A}$ and $\mathbf{B}$. In terms of the corresponding unit vectors $\mathbf{a}=\mathbf{A}/s$ and $\mathbf{b}=\mathbf{B}/s$ the energy per site measured in units of Js^2 (i.e., $w=W/\Lambda Js^2$) is given by

$$w=(\mathbf{a}\cdot\mathbf{b})-\frac{\varepsilon^2}{4}(a_3^2+b_3^2)-\varepsilon\mathbf{h}\cdot(\mathbf{a}+\mathbf{b})\ . \tag{4.12}$$

For the in-plane field of Eq. (4.7) the above energy is minimized when the two spins tilt away from the easy (third) axis, each forming an angle δ with the magnetic field given explicitly by

$$\cos\delta=\frac{2\varepsilon h}{4+\varepsilon^2}\ . \tag{4.13}$$

This canted AFM state is depicted in Fig. 5 together with the vectors $\mathbf{m}=(\mathbf{a}+\mathbf{b})/2$ and $\mathbf{n}=(\mathbf{a}-\mathbf{b})/2$, or

$$\mathbf{m}=(0,\cos\delta,0),\quad \mathbf{n}=(0,0,\pm\sin\delta)\ . \tag{4.14}$$

The $\pm$ choice included in $\mathbf{n}$ reflects the fact that (4.12) is symmetric under exchange of the two spins; if a pair ab minimizes the energy, so does the pair ba.

Now a domain wall on an open chain begins with an ab pair and ends with a ba pair. Therefore the asymptotic values of $\mathbf{m}$ and $\mathbf{n}$ must be given by Eq. (4.14), a fact reproduced very precisely by the calculation in the discrete spin model for any choice of the parameters. On the other hand, the asymptotic expressions of the continuum solution quoted in Eq. (4.11) yield $\cos\delta\approx\varepsilon h/2$, which is consistent with Eq. (4.13) to within terms of order ε^2; and $\sin\delta\approx1$, which would be consistent with Eq. (4.13) only if the condition $\varepsilon h\ll1$ is satisfied, or

$$\frac{g_0\mu_0 H}{2sJ}\ll1\ , \tag{4.15}$$

in addition to $\varepsilon\ll1$. In our standard numerical example we find that $H\ll15\times10^4$ G, a condition that is certainly not stringent for practical purposes. The specific values used in our numerical solution ($\varepsilon=0.1$ and $h=1/2$) fall within the above bounds and explain the success of the continuum approximation. Finally we mention that condition (4.15) excludes strong fields at which a spin-flop transition occurs to a ferromagnetic state, i.e.,

$2\varepsilon h > 4+\varepsilon^2$. In the standard example such a transition takes place at $H = 30\times 10^4$ G.

Our final task is to repeat the preceding analysis for a magnetic field applied along the easy axis:

$$\mathbf{h}=(0,0,h)\ . \tag{4.16}$$

The situation is now more involved in that the usual Néel state remains stable for a sufficiently weak field, while a transition to a canted state occurs when the field exceeds a certain critical value. Actually a detailed examination of the energy function (4.12) reveals that there exist three characteristic field values, namely

$$h_a=\frac{h_b^2}{h_c},\quad h_b=\sqrt{1-\varepsilon^2/4},\quad h_c=\sqrt{1+\varepsilon^2/4}\ , \tag{4.17}$$

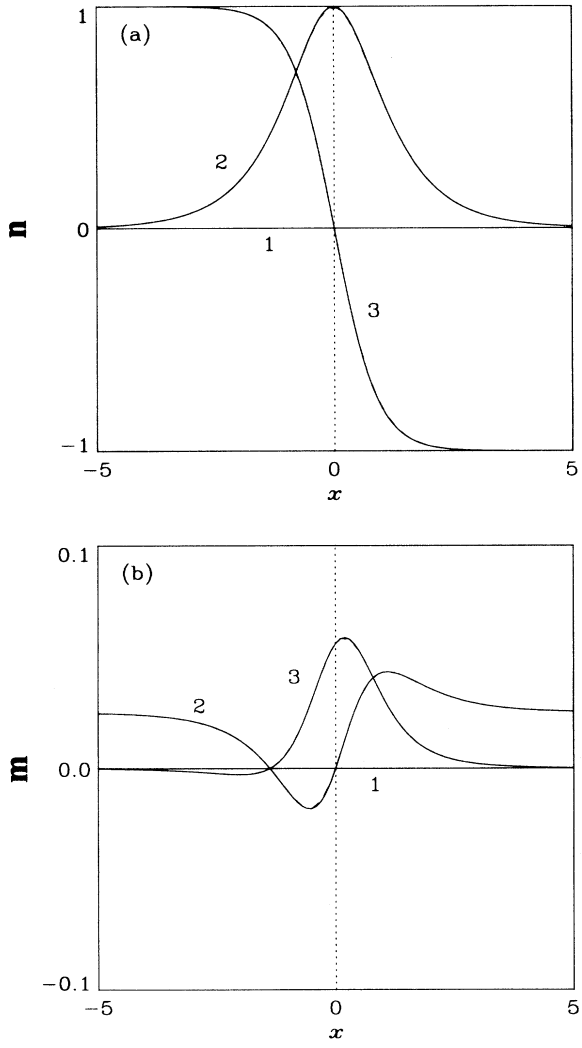

FIG. 4. A static AFM domain wall in the presence of an applied in-plane field $\mathbf{h}=(0,h,0)$. Dashed lines correspond to a numerical calculation with $\varepsilon=0.1$ and $h=1/2$ but are indistinguishable from the solid lines depicting the continuum solution [(4.9) and (4.10)].

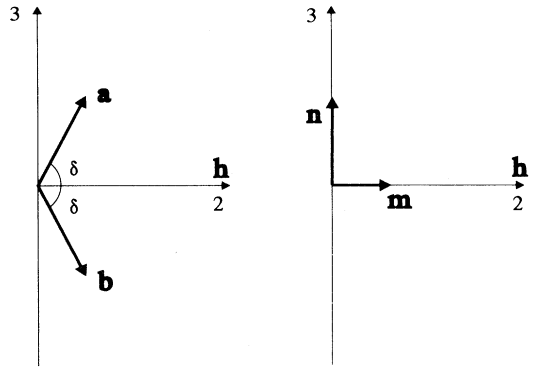

FIG. 5. Schematic illustration of a canted AFM state for an applied in-plane field $\mathbf{h}=(0,h,0)$. The two spins tilt toward the magnetic field each at an angle δ given by Eq. (4.13).

such that $h_a < h_b < h_c$. The usual Néel state ordered along the easy (third) axis is locally stable for $h < h_c$, whereas the canted state of Fig. 6, with

$$\cos\delta=\frac{2\varepsilon h}{4-\varepsilon^2}\ , \tag{4.18}$$

is locally stable for $h > h_a$. Thus there exists an intermediate region, $h_a < h < h_c$, where both states are locally stable, but one of them is globally unstable in the sense that its energy is higher. The two energies coincide at the critical field h_b at which a first-order transition occurs from a Néel state ($h < h_b$) to a canted state ($h > h_b$). However, at small values of ε, the finer details of this transition are suppressed because then $h_a \approx h_b \approx h_c \approx 1$ to within terms of order ε^2. Therefore, within the continu-

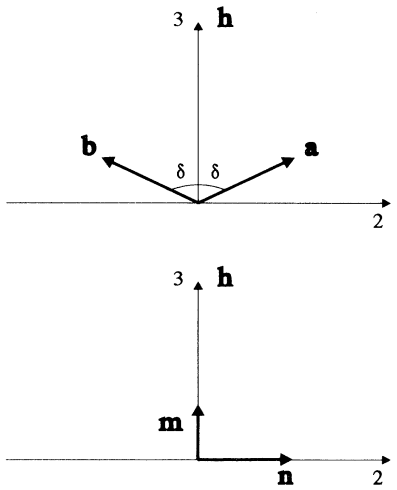

FIG. 6. Schematic illustration of a canted AFM state for a field applied along the easy axis; $\mathbf{h}=(0,0,h)$ with $h > 1$. Each spin forms an angle δ with the easy axis given by Eq. (4.18).

um approximation, the Néel state is stable for $h<1$ and the canted one for $h>1$. Again we mention that a transition to a ferromagnetic state takes place for strong fields, $2\varepsilon h>4-\varepsilon^2$, which lies outside the scope of the present work.

The structure of the classical ground state outlined above determines in large measure the structure of the corresponding domain walls. For the moment, we return to the continuum equation (4.6) applied for the magnetic field (4.16). Ansatz (3.16) is still applicable with the angle θ satisfying the differential equation

$$\theta''=(1-h^2)\cos\theta\sin\theta\ , \tag{4.19}$$

where the expected transition at $h=1$ is made apparent by the fact that the scaling factor $1-h^2$ is positive or negative depending on the region considered.

For $h<1$, a domain-wall solution is given by

$$n_1=0,\quad n_2=\frac{1}{\cosh y},\quad n_3=-\tanh y\ , \tag{4.20}$$

with $y=\sqrt{1-h^2}x$, whereas the magnetization density calculated from Eq. (4.5) reads

$$m_1=0,\quad m_2=\frac{\varepsilon}{2}[h+\sqrt{1-h^2}]\frac{\tanh y}{\cosh y}\ ,$$
$$m_3=\frac{\varepsilon}{2}[h+\sqrt{1-h^2}]\frac{1}{\cosh^2 y}\ . \tag{4.21}$$

The asymptotic values of these fields are consistent with the usual Néel state, as expected for $h<1$; namely, $\mathbf{n}(\mp\infty)=(0,0,\pm1)$ and $\mathbf{m}(\mp\infty)=(0,0,0)$.

The calculated structure resembles very closely the standard AFM wall analyzed in Sec. II, except for a wall broadening caused by the magnetic field and an overall rescaling of the magnetization density. The total moment is now given by

$$\mu_1=0=\mu_2,\quad \mu_3=s\left[1+\frac{h}{\sqrt{1-h^2}}\right]\ , \tag{4.22}$$

and is significantly enhanced in a narrow region near the transition point ($h\sim1$).

As usual, we have performed a straightforward numerical calculation in the discrete model to check the validity of the above solution for $\varepsilon=0.1$ and $h=1/2$. The results of this calculation will not be depicted graphically because the functional form of the solution is the same with that of the standard AFM wall of Sec. II and its agreement with the continuum limit [(4.20) and (4.21)] is now excellent. In fact, the agreement is better than the one obtained for $h=0$ in Fig. 2 thanks to the wall broadening caused by the applied field which brings the discrete solution closer to its continuum approximation. In general, this region of couplings is as favorable as can be; restating the condition $h<1$ in terms of the original field yields

$$\frac{g_0\mu_0 H}{2sJ}<\varepsilon\ , \tag{4.23}$$

which implies that condition (4.15) is automatically enforced when $\varepsilon\ll1$.

On the other hand, the continuum model is expected to be useful also for $h>1$, where the Néel state is turned into the canted state of Fig. 6, as long as condition (4.15) is reasonably well satisfied independently of $\varepsilon\ll1$. The corresponding domain wall is again obtained from Eq. (4.19) taking into account that the scaling factor $1-h^2$ is now negative. It is not difficult to see that the field $\mathbf{n}$ is then given by

$$n_1=0,\quad n_2=-\tanh y,\quad n_3=-\frac{1}{\cosh y}\ , \tag{4.24}$$

with $y=\sqrt{h^2-1}x$, and the magnetization density calculated from Eq. (4.5) by

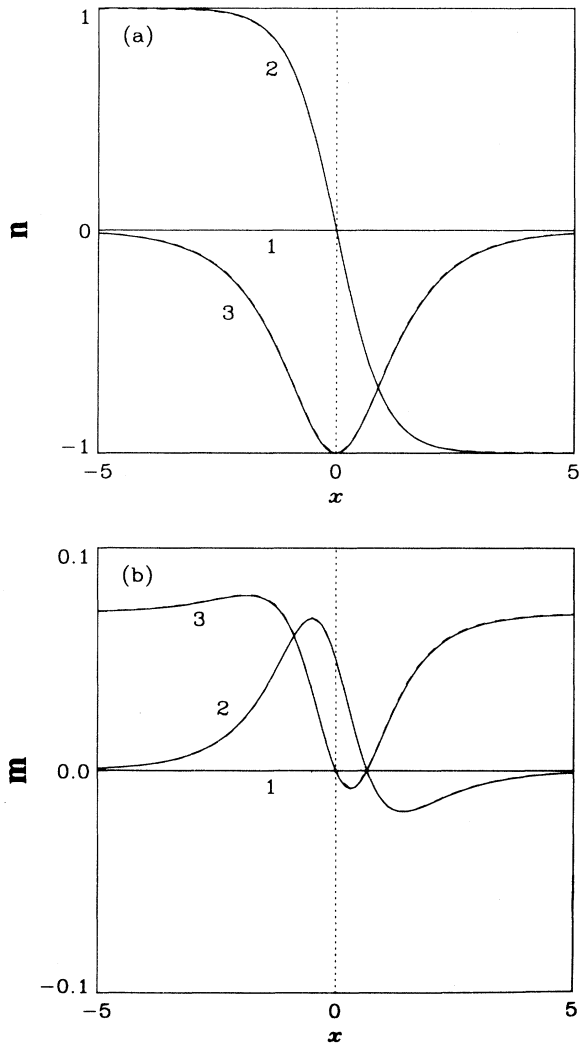

FIG. 7. A static AFM domain wall in the presence of a field applied along the easy axis; $\mathbf{h}=(0,0,h)$ with $h>1$. Dashed lines correspond to a numerical calculation with $\varepsilon=0.1$ and $h=\sqrt{2}$ but are indistinguishable from the solid lines depicting the continuum solution [(4.24) and (4.25)].

$$m_1=0,\quad m_2=\frac{\varepsilon}{2}\left[-h\frac{\tanh y}{\cosh y}+\frac{\sqrt{h^2-1}}{\cosh^2 y}\right],$$
$$m_3=\frac{\varepsilon}{2}\left[h\tanh^2 y-\sqrt{h^2-1}\frac{\tanh y}{\cosh y}\right]. \tag{4.25}$$

The asymptotic values of these fields are consistent with the canted state of Fig. 6 provided that both $\varepsilon \ll 1$ and condition (4.15) are independently satisfied. We have thus performed a numerical calculation in the discrete model for the specific values $\varepsilon=0.1$ and $h=\sqrt{2}>1$, which lie within the above bounds, and the results are compared with the continuum solution [(4.24) and (4.25)] in Fig. 7. The agreement continues to be very good, in analogy with the results for an in-plane field shown in Fig. 4. Again the validity of the continuum approximation becomes progressively questionable for larger values of the applied field.

To summarize, our analytical results in this section are valid for sufficiently weak anisotropy and applied field. They also provide a useful guide for performing straightforward numerical calculations in the discrete spin model for any choice of the parameters, even when the size of the corresponding domain walls reduces to a few lattice spacings. We have confined our attention to static domain walls but the full system (4.3) and (4.4) could be used as a starting point to address questions of dynamics, in analogy with the work of Sec. III, which could then be settled beyond doubt by numerical simulations in the discrete model. Such an analysis will not be pursued further in the present paper but could reveal interesting new effects due to the breakdown of Lorentz invariance caused by the last term in Eq. (4.4).

V. CONCLUDING REMARKS

For a physical interpretation of our results we must now distinguish between the view of a domain wall as a localized soliton in a magnetic chain or as a 1D structure within a 3D magnet. The former view might prove relevant for a semiclassical description of the quantum antiferromagnetic chain with an easy axis anisotropy, where the calculated domain wall may correspond to a collective excitation which is topologically distinct from ordinary magnons. However in such an interpretation one would have to deal with the strong quantum fluctuations known to occur at $D=1$ which modify the Néel state rather significantly. Yet the notion of an AFM domain wall may survive in a quantum chain.[6]

A more feasible direction is to apply the current results to a phenomenological analysis of domain walls within a 3D classical antiferromagnetic continuum. Perhaps the most interesting result in that direction is the nonvanishing total magnetic moment due to the parity-breaking gradient term in the magnetization density **m**. The net moment is roughly equal to the local (staggered) moment s, for each chain in the 3D lattice, and hence small from a macroscopic point of view. Nevertheless it is spread throughout the AFM wall and could possibly be discerned from the local moment by some sort of a magneto-optical experiment; thus providing a signature for the existence of a domain wall within an otherwise magnetically neutral antiferromagnetic background.[9] In this respect, one should recall that the net moment is enhanced when a bias field is applied along the easy axis, albeit at the cost of wall broadening; see Eq. (4.22) and related remarks.

A natural generalization of our work is to consider the antiferromagnetic analogs of ferromagnetic bubbles[1,2] which are essentially 2D topological solitons. FM bubbles are known to exhibit a notorious dynamical behavior which can be summarized by the following two main properties: (i) A FM bubble with a nonvanishing winding number cannot be found in free translational motion, i.e., it is always spontaneously pinned, in the absence of external magnetic-field gradients or other perturbations, and (ii) contrary to naive expectations, a FM bubble tends to move in a direction perpendicular to an applied magnetic-field gradient.

The above properties became especially transparent in a recent study of the ferromagnetic continuum where a direct link was established between topology and dynamics.[10–12] However AFM bubbles would not obey property (i) due to the Lorentz invariance of the underlying nonlinear σ model, and there is no reason to believe that property (ii) is sustained. Yet some remnants of the influence of topology on dynamics should persist, as is evident from independent studies in the context of the nonlinear σ model where bubbles display an unusual scattering behavior; for instance, two bubbles scatter at 90° during a head-on collision.[13] It is clearly desirable to elucidate such a behavior in the context of an antiferromagnet.

Finally, some aspects of the existing theory of domain walls and bubbles in weak ferromagnets may have to be revised in view of the current findings. As mentioned already, the work presented in this paper was a reaction to the theoretical analysis of weak ferromagnets reviewed in Ref. 3.

ACKNOWLEDGMENTS

I am grateful to Igor and Victor Bar'yakhtar for providing me with a copy of Ref. 3 and for a number of related discussions. The work was supported in part by two grants from the EEC (SCI-CT-91-0705 and CHRX-CT93-0332) and by a travel grant from the Voroni Foundation (Voicotsa 1994).

[1] A. P. Malozemoff and J. C. Slonczewski, *Magnetic Domain Walls in Bubble Materials* (Academic, New York, 1979).

[2] T. H. O'Dell, *Ferromagnetodynamics, the Dynamics of Magnetic Bubbles, Domains and Domain Walls* (Wiley, New York, 1981).

[3] V. G. Bar'yakhtar, M. V. Chetkin, B. A. Ivanov, and S. N. Gadetskii, *Dynamics of Topological Magnetic Solitons—Experiment and Theory* (Springer-Verlag, Berlin, 1994).

[4]I. V. Bar'yakhtar and B. A. Ivanov, Sov. J. Low. Temp. Phys. **5**, 361 (1979); Solid State Commun. **34**, 545 (1980).
[5]H. J. Mikeska, J. Phys. C **13**, 2913 (1980).
[6]F. D. M. Haldane, Phys. Lett. A **93**, 464 (1983); Phys. Rev. Lett. **50**, 1153 (1983); J. Appl Phys. **57**, 3359 (1985).
[7]I. Affleck, J. Phys. Condens. Matter **1**, 3047 (1989).
[8]N. L. Schryer and L. R. Walker, J. Appl. Phys. **45**, 5406 (1974).
[9]Such a possibility was suggested to the author by Victor Bar'yakhtar.
[10]N. Papanicolaou and T. N. Tomaras, Nucl. Phys. B **360**, 425 (1991).
[11]N. Papanicolaou, Physica D **74**, 107 (1994); Phys. Lett. A **186**, 119 (1994).
[12]N. Papanicolaou and W. J. Zakrzewski, Physica D **80**, 225 (1995).
[13]R. A. Leese, M. Peyrard, and W. J. Zakrzewski, Nonlinearity **3**, 773 (1990).